Journal of Geochemical Exploration 188 (2018) 229–239

Contents lists available at ScienceDirect

Journal of Geochemical Exploration

journal homepage: www.elsevier.com/locate/gexplo

Identification of sandstones above blind uranium deposits using multivariate statistical assessment of compositional data, Athabasca Basin, Canada

Shishi Chen[a,*], Keiko Hattori[a], Eric C. Grunsky[b,c]

[a] Dept. of Earth and Environmental Sciences, University of Ottawa, Ottawa, Ontario K1N 6N5, Canada
[b] China University of Geosciences, Beijing, 29 Xueyuan Road, Beijing 100083, China
[c] Dept. of Earth and Environmental Sciences, University of Waterloo, Waterloo, Ontario N2L 3G1, Canada

ARTICLE INFO

Keywords:
Footprint
Lithogeochemistry
Multivariate statistical analysis
Exploration
Uranium
Unconformity
Machine learning

ABSTRACT

The Athabasca Basin in northern Saskatchewan, Canada, hosts the world's largest high-grade U resources near the unconformity between sandstones and underlying crystalline basement rocks. Finding U deposits is difficult in the interior of the Athabasca Basin where the sandstone cover can reach 1400 m. This study uses the lithogeochemistry of sandstones obtained from drill cores to identify elements associated with U using principal component analysis (PCA) from three areas; samples directly above the Phoenix U deposit, those in Denison Mine's Wheeler River property and background areas in the basin. The sandstone data from the Wheeler River property shows that U is positively associated with Y-Cu-Zn-Na-W-Co-Ni-B-Mg-HREEs-Cr-Sc-Mo-V-LREEs due to uraniferous hydrothermal alteration. In contrast, the principal components derived from the lithogeochemistry of sandstones far from known mineralization in the basin shows that U is positively associated with Th-Ti-Zr-Hf, suggesting that U is hosted in refractory detrital minerals. Linear discriminant analysis (LDA) and random forest (RF) analysis based on principal components of elements associated with U show three classes of sandstones with clear discrimination between samples; those above the Phoenix ore (Class Phoenix), in the Wheeler River (Class Wheeler River), and regional background (Class Regional Background). The class Phoenix contains most of the sandstone samples overlying the Phoenix deposit and a few samples in the Wheeler River property. This study shows that PCA, LDA and RF are able to detect geochemical footprints of uraniferous hydrothermal alteration > 500 m from the ore and differentiate sandstones spatially associated with the mineralization from those in barren areas. Based on the performance of the two discrimination methods, we suggest that RF is a preferred method as it better differentiates altered sandstones from regional background samples. The classification analysis used in this study may be useful in U exploration in Athabasca Basin and other sedimentary basins.

1. Introduction

Many U deposits in the Athabasca Basin occur along the regional unconformity between sandstones and the crystalline basement. The majority of the known U deposits, including the world's largest McArthur River deposit, are located in the eastern margin of the basin (Fig. 1) where the sandstones are relatively thin (< 400 m) compared to the interior of the basin where they are up to 1400 m thick. Geophysical methods, such as radiometric prospecting and electromagnetic surveys, have played important roles in the discoveries of U deposits. However, the thick sandstones pose difficulties for geophysical surveys for U exploration. For example, high gamma rays from the Wolverine Point Formation of ~186 m thick (Ramaekers, 1979) may yield misleading exploration targets. Many deposits are spatially associated with conductive graphitic pelites in the basement, but there are many barren graphitic pelites. In addition, several newly discovered deposits are not associated with graphitic conductors (e.g., Centennial deposit; Reid et al., 2014). Therefore, electromagnetic surveys may not be able to detect these deposits. This prompted a study to identify the geochemical signatures of sandstones overlying buried U deposits. Previous studies reported that concentrations of selected elements, such as Pb, U, Ni, As, REEs and Co, are anonymously high above and close, up to 200 m, to some deposits and prospects (Sopuck et al., 1983; Hoeve and Quirt, 1984; Earle and Sopuck, 1989; Jefferson et al., 2007). Recent studies of sandstone lithogeochemistry suggests that the anomalies extend much farther (Dann et al., 2014; Wright et al., 2015; Guffey et al., 2015; Chen et al., 2017). This study tests the possibility that multivariate statistical methods can distinguish altered sandstones above deeply-buried U deposits from those in barren areas.

We selected the Denison Mine's Wheeler River property in the

* Corresponding author.
E-mail address: schen162@uottawa.ca (S. Chen).

https://doi.org/10.1016/j.gexplo.2018.01.026
Received 10 October 2017; Received in revised form 22 January 2018; Accepted 29 January 2018
Available online 31 January 2018
0375-6742/ Crown Copyright © 2018 Published by Elsevier B.V. All rights reserved.

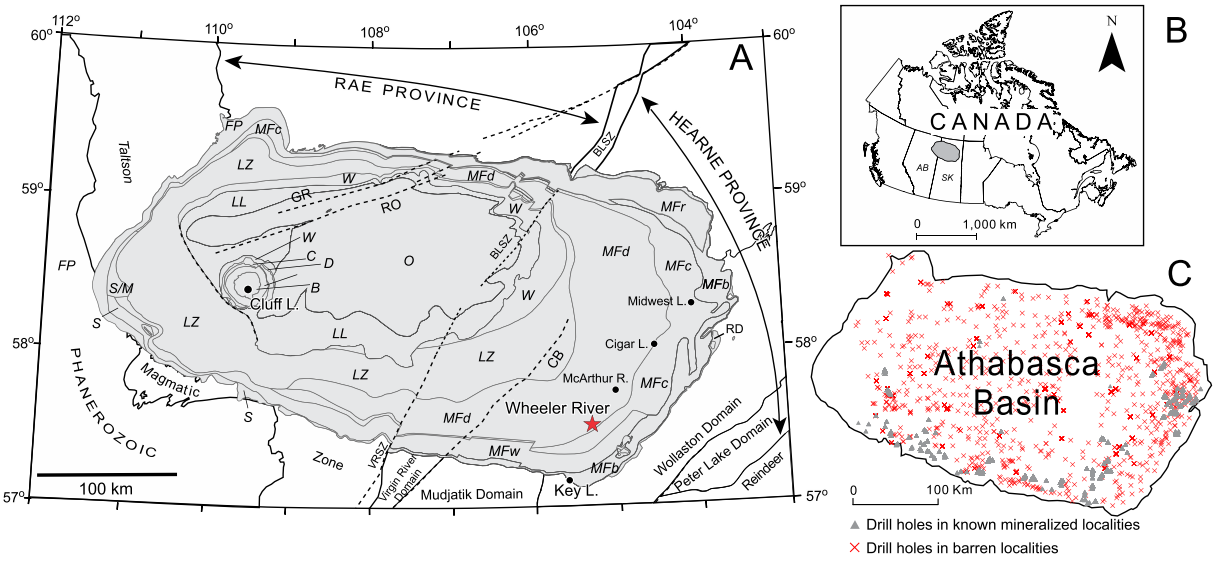

Fig. 1. A. The simplified geological map of the Athabasca Basin (shaded area), Saskatchewan, Canada, after Jefferson et al. (2007) and Bosman et al. (2012) and the locations of selected major U deposits (solid circles). Grey lines denote boundaries of stratigraphic units. Black lines denote boundaries of geological domains. Dashed lines denote major basement structures. The Wheeler River property (solid red star) is underlain by the basement rocks of the Wollaston Domain close to the contact with the Mudjalik Domain. Major shear zones: BLSZ = Black Lake Shear Zone, CB = Cable Bay, GR = Grease River Shear Zone, H = Harrison Shear Zone, RO = Robbilard, VRSZ = Virgin River Shear Zone, H = Harrison Shear Zone. Formations: B = basement; FP = Fair Point Formation; S = Smart Formation; S/M = undifferentiated Smart and/or Manitou Falls; RD = Read Formation; MF = Manitou Falls Formation (b = Bird Member; w = Warnes Member; c = Collins Member; d = Dunlop Member); LZ = Lazenby Lake Formation; W = Wolverine Point Formation; LL = Locker Lake Formation; O = Otherside Formation; D = Douglas Formation. C = Carswell; F/O = undivided Fair Point to Otherside Formations. B. The location of the Athabasca Basin in Canada. AB = Alberta; SK = Saskatchewan. C. Locations of the diamond drill hole (DDH) collars in Athabasca Basin used in the lithogeochemical analysis.
(From Wright et al., 2015)

eastern margin of the Athabasca Basin because it hosts the Phoenix U deposit along the unconformity and the basement-hosted Gryphon U deposit. This study applies principal component analysis (PCA), linear discriminant analysis (LDA) and random forest (RF) analysis to lithogeochemical data of sandstones from diamond drill cores. The use of PCA simplifies the variation and relationships of the data in a reduced number of dimensions (Neff, 1994), each of which is commonly linked to specific geochemical/geological processes, such as alteration and mineralization (e.g., Chandrajith et al., 2001; Grunsky, 2010; Cheng et al., 2011; Zuo, 2011; Grunsky et al., 2014; Chen et al., 2016, 2017). We use R (variables = elements)-Q (observations = samples) mode PCA to determine element assemblages associated with U in sandstones in Wheeler River property. The element assemblages are compared with those in sandstones from barren areas (regional background data) in the Athabasca Basin. Finally, discriminant analysis was carried out to differentiate the sandstone lithogeochemistry from mineralized properties versus barren areas. Discriminant analysis commonly uses element concentrations as variables (e.g., Clarke et al., 1989; Chork and Rousseeuw, 1992; Mao et al., 2016). The use of principal components (PCs) as variables of classification algorithms is advantageous because PCs likely reflect processes responsible for compositional variability (Grunsky et al., 2014; McKinley et al., 2017). Therefore, this study uses LDA and RF based on the scores of PCs to achieve better discrimination of sandstone lithogeochemistry in the area with U deposits and those in barren areas in the Athabasca Basin.

2. Study area

Unconformity-related uranium deposits in the Athabasca Basin are characterized by extensive hydrothermal alteration halos overprinting the diagenetic minerals of the sandstones and the metamorphic minerals of the basement rocks (Hoeve and Quirt, 1984; Kotzer and Kyser, 1995). Common alteration minerals include kaolinite, illite, chlorite, dravitic tourmaline, hematite and aluminum phosphate-sulphate (APS) minerals (Hoeve and Quirt, 1984; Kotzer and Kyser, 1995; Jefferson et al., 2007; Adlakha and Hattori, 2015). Alteration halos commonly extend several hundred meters from major deposits (Hoeve and Quirt, 1984; Kotzer and Kyser, 1995).

The Phoenix deposit in the Wheeler River property occurs along the unconformity, at a depth of approximately 400 m below the present day surface (Fig. 2). At present, it is one of the largest undeveloped U deposit in the Athabasca Basin with indicated resources of 70.2 M lb U_3O_8 at a grade of 19.1% U_3O_8 (Roscoe, 2015). The Gryphon deposit was discovered in 2014, approximately 3 km northwest to the Phoenix deposit (Fig. 2). It is hosted in basement rocks, approximately 35 m below the unconformity and currently estimated to contain inferred resources of 43 M lb U_3O_8 at a grade of 2.3% U_3O_8 (Denison Mines Corp., 2017). Alteration in the study area is typical unconformity-associated style including dravitization, chloritization and illitization of sandstones and basement rocks. The major structural feature of the basement rocks in the property is the NE-SW trending WS reverse fault which dips to the southeast and lies along the southeastern margin of a quartzite ridge in the basement (Fig. 2). The major U bodies are adjacent to this WS fault. The WS fault and its splay structures likely acted as conduits of mineralizing fluids (Roscoe, 2015; Chen et al., 2017).

The Athabasca Group sandstones are ~400 m thick in the area except for above the aforementioned quartzite ridges that was a paleotopographic high where the overlying sandstones thin to ~200 m (Fig. 2). The Athabasca Group sandstones in the eastern part of the basin consist of the basal conglomeratic Read Formation (RD) and three members of the Manitou Falls Formation; the conglomeratic and heavy mineral-bearing Bird (MFb), sandy Collins (MFc) and uppermost clay intraclast-bearing Dunlop (MFd) members. The lithology is described in detail by Ramaekers et al. (2007).

3. Data sources

All lithogeochemical data of sandstones in the Wheeler River property and overlying Phoenix deposit were analyzed at the Saskatchewan Research Council (SRC) for Denison Mines Corporation after near-total digestion using the mixture of HF, HNO_3 and HCl (analytical code 3AMS). Boron concentrations were determined by

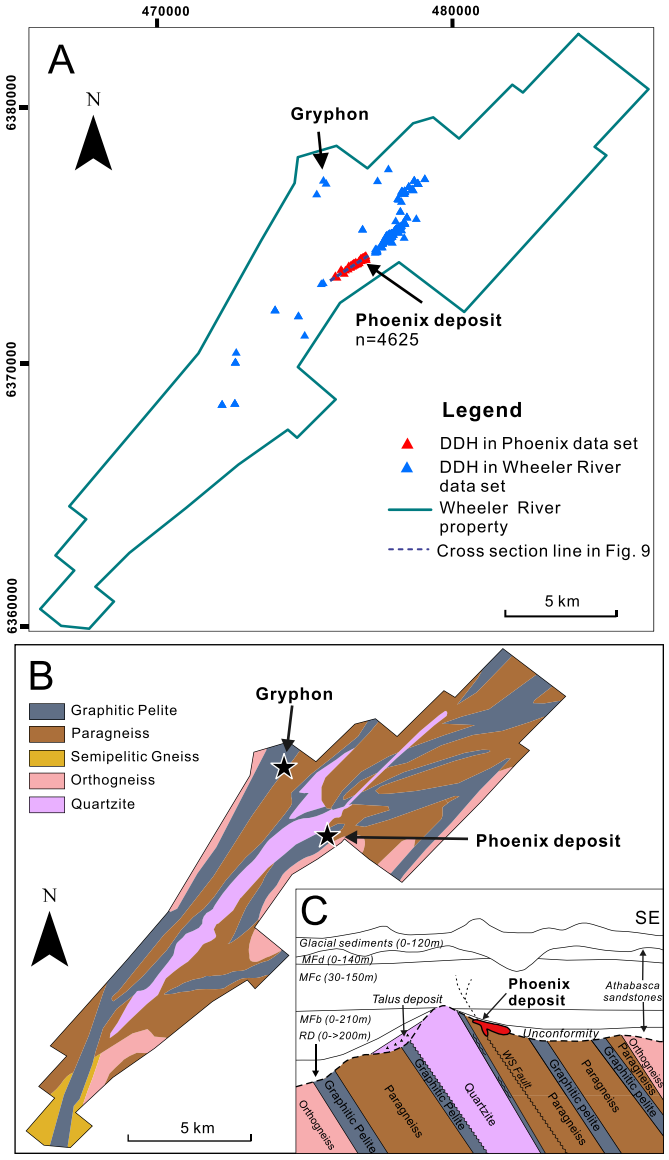

Fig. 2. A. Locations of DDH collars in Wheeler River Property. Eastings and northings are in meters in Zone 13 of NAD 83. The surface projection of the Gryphon deposit is shown with an arrow. The dark blue dashed line represents the location of the vertical section shown in Fig. 9C and D. B. Basement geological map of the Wheeler River property at the unconformity (after Roscoe, 2015). C. NW-SE schematic cross-section of the Phoenix deposit (modified after Gamelin et al., 2010). Note that the Phoenix deposit contains several ore pods. (For interpretation of the references to color in this figure legend, the reader is referred to the web version of this article.)

inductively coupled plasma optical emission spectrometry after fusion of rock pulps with a mixture of Na_2O_2 and $NaCO_3$. Details on the analytical methods and the quality control procedures are described by Roscoe (2015). Total Fe contents are expressed as Fe_2O_3 (T). The data contains the abundances of Al_2O_3, Ag, B, Ba, Be, CaO, Co, Cd, Ce, Cr, Cu, Dy, Er, Eu, Fe_2O_3, Ga, Gd, Hf, Ho, K_2O, La, Li, MgO, MnO, Mo, Na_2O, Nb, Nd, Ni, P_2O_5, Pb, Pr, Sc, Sm, Sn, Sr, Ta, Tb, Th, TiO_2, U, V, W, Y, Yb, Zn, and Zr. In this study, light rare earth elements (LREEs) include La, Ce, Nd, Sm, Eu, and Gd, and heavy REEs (HREEs) are Dy, Er, Ho and Yb. The results of sandstone samples from diamond drill holes (DDHs) far from the Phoenix deposit (drill collars > 500 m of the surface projection of Phoenix ore body) in the Wheeler River property are named as "Wheeler River data set". It contains 6305 sandstone samples from 157 DDHs. Among them, 535 sandstone samples are from MFd, 2144 from MFc, 1470 from MFb and 2156 from RD. The compositional data of sandstones directly overlying the Phoenix U deposit (drill core collars < 500 m of the surface projection of Phoenix ore body, Fig. 2) are defined as "Phoenix data set". This data set contains 4625 samples from 141 DDHs. The statistical summary of 'Phoenix data set' is provided in Chen et al. (2017).

Wright et al. (2015) compiled sandstone lithogeochemical data from Saskatchewan Government assessment records between 2000 and 2014 from the entire Athabasca Basin, including both mineralized and non-mineralized areas. This study uses sandstones in unmineralized areas as the "regional" data set (n = 2175). They are located far (> 5 km, Fig. 1) from known U deposits. A statistical summary of each data set is shown in Table 1.

4. Methodology

4.1. Statistical treatments before multivariate analysis

The raw data was processed before applying multivariate analysis. First, elements that show values below or equal to the detection limits in > 90% of the samples in a data set were removed. Silver was removed during this process. Second, missing values or values lower than the detection limits were replaced using a method of k-nearest neighbors (impKNNa) that provides reliable estimates of replacement values (Hron et al., 2010). This step was implemented using the "robCompositions" package of the R program (Templ et al., 2010). In this study, samples with missing values comprised < 5% of the total database and missing values for Y, REEs and U were < 2% of the total. We consider that any potential bias related to imputed values insignificant compared to the geochemical patterns reported in this study. This study uses centered log ratios to eliminate the closure problem (all components sum to a constant value and thus are not independent; Aitchison, 1986).

4.2. Multivariate statistical techniques

This study uses R-Q mode PCA, which calculates variable and object loadings simultaneously and thus displays the relationships between samples and elements at the same scale. To evaluate the affinity of the elements with U, Euclidean distance (D) of each element (X) to U in the n-dimensional space of selected PCs is calculated below. This method is one of the most frequent choices to measure distance between the observations or variables (Templ et al., 2008).

$$D_x = \sqrt{\sum_{i=1}^{n} (X_i - U_i)^2}$$

This study implemented LDA using the lda procedure of "MASS" package by Venables and Ripley (2002) of the R program (R Core Team, 2013). LDA is a supervised classification method to distinguish between classes of samples by finding linear combination of variables that best separate the classes (Carranza, 2008; Filzmoser et al., 2012). To achieve better discrimination, an additional PCA is conducted on the elements that are positively and inversely associated with U, along with an analysis of variance (ANOVA) applied to the PC scores to determine which PCs are best at discriminating between the classes. Cross validation was used for accuracy estimates from the lda procedure.

Random forest (RF), originally developed by Breiman (2001), is a

Table 1
Univariate statistical summary of Regional and Wheeler River data sets.

Element	Unit	Regional (n = 2175)					Wheeler River (n = 6305)				
		Min	1st Qu.	Med	3rd Qu.	Max	Min	1st Qu.	Med	3rd Qu.	Max
Al_2O_3	wt%	0.05	0.5	0.8	1.7	33	0.14	1.1	1.7	2.4	32
B	ppm	N/A	N/A	N/A	N/A	N/A	3	44	88	230	12,800
Ba	ppm	0.5	10	14	20	1590	3	8	10	13	267
Be	ppm	< 0.1	0.1	0.1	0.2	11	N/A	N/A	N/A	N/A	N/A
Ca	wt%	< 0.01	0.01	0.02	0.03	24	< 0.01	0.01	0.02	0.02	1.4
Ce	ppm	0.5	17	23	34	1770	9	27	35	48	513
Co	ppm	0.02	0.1	0.2	0.3	44	0.05	0.32	0.5	0.88	101
Cr	ppm	< 1	2.5	5	9	170	2	8	11	16	297
Cu	ppm	< 0.1	0.5	0.5	0.8	82	0.2	1	2.1	4.1	634
Dy	ppm	0.1	0.4	0.6	1	63	0.34	0.74	0.92	1.2	36
Er	ppm	0.04	0.22	0.32	0.54	31	0.2	0.4	0.51	0.67	15
Eu	ppm	0.02	0.16	0.22	0.35	30	0.1	0.24	0.3	0.4	8.8
Fe_2O_3(T)	wt%	0.02	0.05	0.11	0.43	19	0.02	0.07	0.21	0.93	21
Ga	ppm	< 0.1	0.5	0.6	1.1	41	0.3	1.8	2.4	3.2	49
Gd	ppm	< 0.1	0.82	1.21	1.9	138	0.8	1.6	2.1	2.9	37
Hf	ppm	< 0.1	1.1	2	4	182	0.7	3.3	4.8	6.7	39
Ho	ppm	< 0.02	0.08	0.11	0.19	13	0.06	0.13	0.17	0.23	7.2
K_2O	wt%	0.004	0.03	0.09	0.2	7.9	0.005	0.047	0.22	0.47	2.33
La	ppm	< 1	8	10	15	901	4	13	17	24	288
Li	ppm	0.5	3	6	13	551	1	5	7	10	262
MgO	wt%	0.003	0.01	0.02	0.05	9	0.005	0.09	0.17	0.26	9.08
MnO	wt%	< 0.001	0.001	0.001	0.002	0.17	0.001	0.001	0.003	0.003	0.06
Mo	ppm	0.02	0.08	0.12	0.22	54	0.04	0.12	0.18	0.26	127
Na_2O	wt%	< 0.01	0.01	0.01	0.02	1.9	0.005	0.005	0.01	0.03	1.56
Nb	ppm	< 0.1	0.6	1	2.1	69	0.3	1.7	2.9	4.6	30.4
Nd	ppm	0.7	6.1	8.2	13	829	4.3	9.8	13.2	18.1	212
Ni	ppm	< 0.1	0.4	0.6	1.2	166	0.4	3.3	5.4	9.2	405
P_2O_5	wt%	0.001	0.01	0.01	0.03	17	0.005	0.019	0.03	0.044	0.39
Pb	ppm	0.36	3.3	3.2	4.4	135	0.79	0.79	3.15	4.09	998
Pr	ppm	0.2	1.8	2.4	3.6	181	1.4	3	4	5.5	66
Rb	ppm	N/A	N/A	N/A	N/A	N/A	0.1	0.8	2.4	4.6	54.9
Sc	ppm	N/A	N/A	N/A	N/A	N/A	0.1	0.5	0.7	0.9	23.2
Sm	ppm	0.1	1	1.4	2.2	193	0.8	1.7	2.3	3.2	50.5
Sn	ppm	< 0.02	0.1	0.18	0.4	14	0.01	0.25	0.38	0.63	26.7
Sr	ppm	2	45	67	107	1950	12	60	108	175	1380
Ta	ppm	N/A	N/A	N/A	N/A	N/A	< 0.1	0.2	0.3	0.5	6.6
Tb	ppm	< 0.02	0.08	0.12	0.19	13	0.06	0.15	0.19	0.25	6.04
Th	ppm	0.45	2.3	3.4	6.5	1130	1.64	6.56	11.5	21	210
TiO_2	wt%	0.007	0.02	0.04	0.09	5.05	0.013	0.066	0.11	0.17	1.44
U	ppm	0.24	0.5	0.72	1.2	207	0.45	1.23	1.72	2.67	1800
V	ppm	0.3	1.4	2.4	5.3	661	0.6	4.7	7.8	12.6	482
W	ppm	0.02	0.05	0.1	0.25	10.2	0.1	0.2	0.4	0.6	154
Y	ppm	0.4	1.84	2.68	4.6	324	1.6	3.4	4.4	6.1	185
Yb	ppm	0.05	0.05	0.21	0.4	21.4	0.21	0.43	0.54	0.71	9.7
Zn	ppm	0.2	1	2	3	344	1	2	3	4	692
Zr	ppm	1.7	38.7	69.2	145	7000	19	107	153	221	1360

N/A = not analyzed.

classification and regression method based on the use of decision trees and bootstrapping. Analytics Vidhya Content team (2016) provides the description of decision trees and RF. In this method, each decision tree uses a training subset that is randomly chosen and then replaced for a number of times equal to the number of trees in the ensemble (referred to "bootstrapping"). Approximately 2/3 of the training samples are employed for prediction (in bag samples) while the remaining roughly 1/3 of the training samples are left out of the bootstrap samples for validation (*oob*, out-of-bag samples). For each of the bootstrap samples, an unpruned classification or regression tree is grown. At each node, rather than choosing the best split among all variables, a random selection of variables is made and the best split from among those variables are chosen. Prediction can be achieved by aggregating the majority votes of the trees for classification and *oob* accuracy is used to measure the prediction accuracy of RF. Mean Decrease Gini is used to measure variable importance based on the Gini impurity index for the calculation of splits during training. In this study, supervised mode RF is conducted using R package "randomForest" by Liaw and Wiener (2002). The number of variables available for each tree (*mtry*) is set to the square root of the total number of variables following the recommendation of Harris and Grunsky (2015) and the total number of trees (*ntree*) is set through experimentation to achieve lowest prediction errors during the reasonable computation time.

5. Results

5.1. Principal component analysis

5.1.1. Wheeler River data set

Principal components 1 and 2 (PC1, PC2) account for a large part of the variability (a total of 44.4%, 26.8% for PC1 and 17.6% for PC2, Supplementary Table A.1.a) in the Wheeler River data set. Therefore, these PCs reflect the major processes responsible for the variability in lithogeochemistry of the sandstones. PC1 accounts for the majority of the U variability, 65.2% (Supplementary Table A.1.c). The U variability in other PCs is much smaller (< 3.6% in each PC) than that in PC1, therefore, other PCs are not as significant for the distribution of U as PC1. Uranium is positively associated with REEs-Y-Cu-Na-Zn-W-Co-Ni-

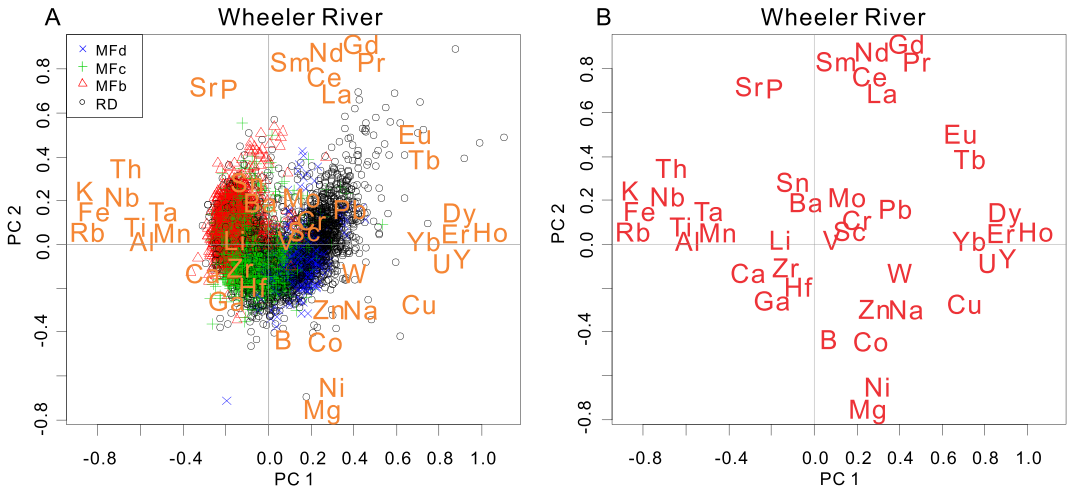

Fig. 3. Biplot of PC1 vs. PC2 of Wheeler River data set, after log centered transformation. For the clarity of diagrams, elements are shown as faded font in 3A and separately shown in 3B. Samples with relatively high contents of a given element plot close to the position of the element.

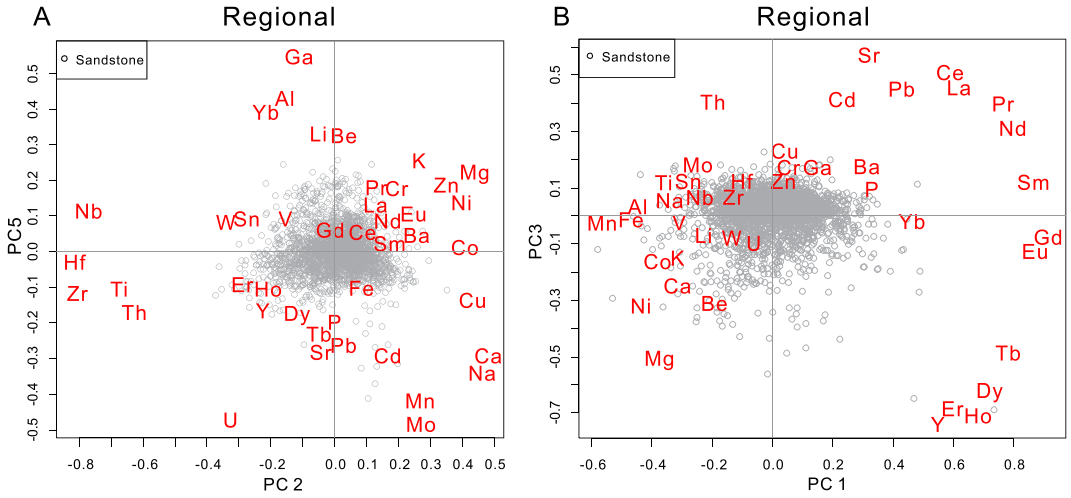

Fig. 4. A. Biplot of PC2 vs. PC5 of regional background data set, after log centered transformation. B. Biplot of PC1 vs. PC3 of regional background data set.

B-Mg-Pb-Sc-Mo and inversely with K-Rb-Fe-Th-Nb-Ti-Mn-Al-Ta-Sr-P-Sn-Li-Ba in PC1 (Fig. 3). The concentrations of U-associated elements are high in RD and MFd rocks (Fig. 3A) as most of the RD and many MFd samples are plotted along the positive PC1 axis. Most of the elements positively associated with U, such as Y, Sc and W, are not mobile at low temperatures and their association therefore reflects hydrothermal processes. The positive association of U and Zr-Hf-Ca-Ga is observed in PC2 but the loadings of U, Zr, Hf, Ca and Ga in PC2 are small, being close to the origin (Fig. 3, Supplementary Table A.1.b). Therefore, this association is very weak.

PC3 accounts for the major variabilities of Zr (71.3%), Hf (72.3%), Ti (41.8%) and a very small part of U variability (0.2%) (Supplementary Table A.1.c). Positive association of Zr, Hf, Ti and U in this PC3 indicates that small amount of U may be hosted by refractory detrital minerals, such as zircon and Ti oxides. PC4, PC5 and PC7 all show positive association of Fe and U (Supplementary Table A.1.b, c) and account for 2%, 5.5% and 2.6% of total Fe variability and 3.6%, 0.7% and 1.6% of total U variability, respectively. The data suggest that a minor amount of U may be adsorbed to Fe oxides/hydroxides. These PCs suggest that U is mostly associated with elements introduced to sandstones by hydrothermal activity, and that very minor fractions of U are hosted by refractory detrital minerals or Fe oxide/hydroxides formed at low temperatures.

5.1.2. Regional data set

The regional data set shows that PC2 and PC5 account for the majority of U variability, 32.8% in total (Supplementary Table A.2.c). The biplot of the two PCs shows that U is strongly associated with HREEs-Y-Th-Ti-Zr-Hf and intermediately with Fe-Cd-Mn-Cu-Na-Mo-Ca (Fig. 4A). PC1 and PC3 account for the major part of variability of REEs + Y (62.7%–84.6%, Supplementary Table A.2.c), but these elements are not associated with U (Fig. 4B).

5.2. Linear discriminant analysis

To identify sandstones affected by uraniferous hydrothermal activity, linear discriminant analysis was conducted based on elements identified in PC1 and PC2 of the Wheeler River data set and their affinity with U were calculated based on the distances to U on the PC1 vs. PC2 space.

Table 2 lists distances of the elements to U in PC1, PC2 and the Euclidean distances of elements to U in the PC1 vs. PC2 space separately. Using the degrees of affinity of elements with U, there appears to be three groups of elements: strongly positive associated with U in PC1 and PC2 (Element Assemblage A), associated with U in only PC2 (Element Assemblage B), and inversely associated with U in PC1 and PC2 (Element Assemblage C).

Table 2
Affinity of each element with U, based on its Euclidean distance to U in PC1 vs. PC2 space, distance to U in PC1 and distance to U in PC2.

Elemental assemblage	Element	Euclidean distance to U	Distance to U in PC1	Distance to U in PC2
A	Y	0.1	0.08	0.06
	Er	0.13	0.09	0.1
	Yb	0.14	0.08	0.11
	Ho	0.15	0.06	0.14
	Cu	0.22	0.11	0.19
	Dy	0.23	0.08	0.22
	W	0.41	0.41	0.05
	Na	0.43	0.38	0.21
	Zn	0.46	0.41	0.22
	Pb	0.51	0.44	0.25
	Tb	0.53	0.09	0.52
	Eu	0.6	0.13	0.59
	Cr	0.65	0.62	0.2
	Co	0.65	0.55	0.36
	Sc	0.66	0.65	0.15
	V	0.69	0.69	0.1
	Mo	0.7	0.66	0.25
	Ni	0.77	0.52	0.57
	B	0.82	0.74	0.35
	Mg	0.88	0.57	0.68
	La	0.98	0.48	0.85
	Ce	1.03	0.53	0.88
	Gd	1.04	0.49	0.94
	Pr	1.07	0.54	0.93
	Nd	1.08	0.54	0.94
	Sm	1.16	0.66	0.96
B	Zr	0.95	0.95	0.02
	Hf	0.95	0.95	0.02
	Ga	1.03	1.01	0.17
	Ca	1.12	1.12	0.04
C	Ba	0.90	0.86	0.28
	Li	0.98	0.98	0.1
	Sn	1.16	0.93	0.31
	P	1.27	1	0.79
	Ta	1.33	1.31	0.23
	Sr	1.37	1.12	0.8
	Al	1.41	1.41	0.1
	Ti	1.46	1.45	0.16
	Mn	1.46	1.45	0.17
	Nb	1.53	1.51	0.27
	Th	1.55	1.49	0.43
	Fe	1.65	1.63	0.24
	Rb	1.67	1.66	0.22
	K	1.69	1.68	0.26

Elemental Assemblage A = elements positively associated with U in PC1. Elemental Assemblage B = elements positively associated with U in only PC2. Elemental Assemblage C = elements inversely associated with U in PC1. Note Sc, Sn, Rb, Ta and B are not used in the following classifications because the concentrations of these elements are not available in all data sets.

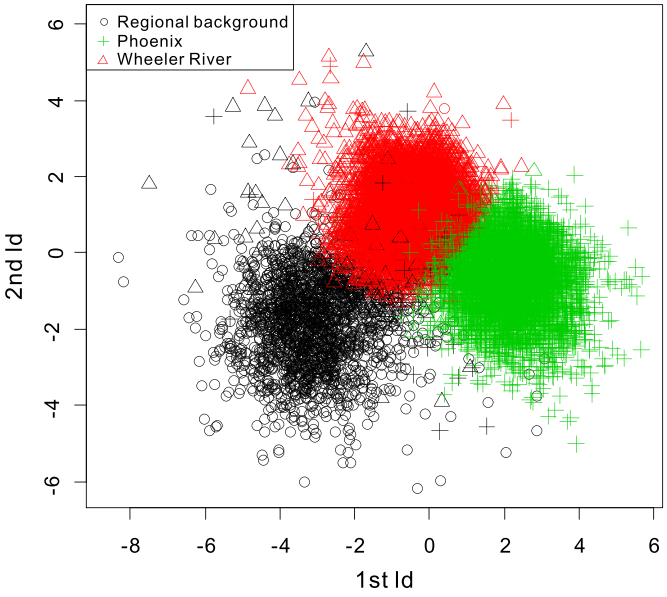

Fig. 6. LDA using the first 8 dominant PCs, ld = linear discriminant. For each sample, the color represents the predicted classification and the symbol represents the actual classification.

Table 3
Predictive accuracies derived from the linear discriminant analysis.

Data sets	Predicted			Accuracy rate	Total accuracy rate
	Regional background	Phoenix	Wheeler River		
Regional background	2051	8	116	94.3%	95.5%
Wheeler River	109	156	6040	95.6%	
Phoenix	37	4414	168	95.8%	

Wilk's Lambda = 0.02; $p < 0.001$.

Principal component analysis was also applied to the elements that are positively and inversely associated with U in PC1 and PC2 (Element assemblages A and C in Table 2) which represents the major signature of hydrothermal activities in the research area. The result of an ANOVA shows that the F values of the 8 PCs, PC3, PC6, PC2, PC13, PC11, PC1, PC14, PC4, are very high, > 400 (Fig. 5). Therefore, LDA using these 8 PCs may yield best discrimination. The LDA yielded three classes of

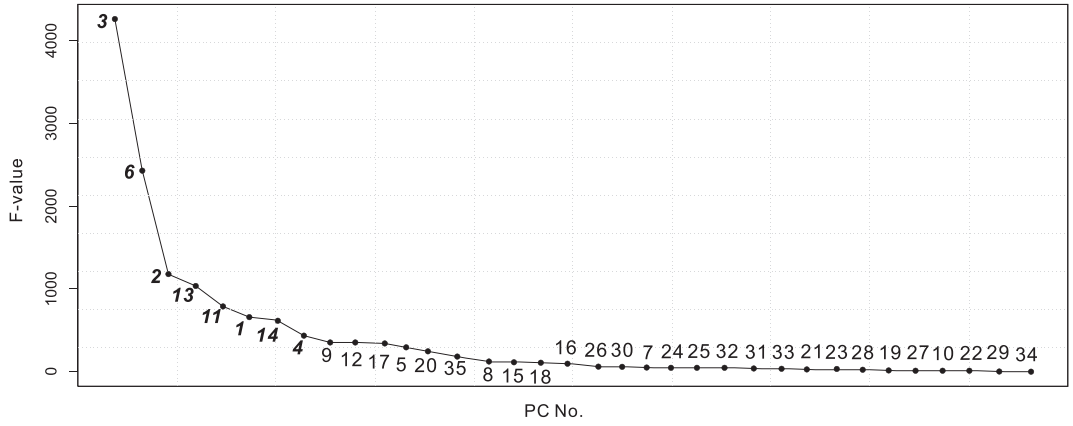

Fig. 5. F values of the PCs. PC3, PC6, PC2, PC13, PC11, PC1, PC14 and PC4 have high F values and they were used as variables in LDA.

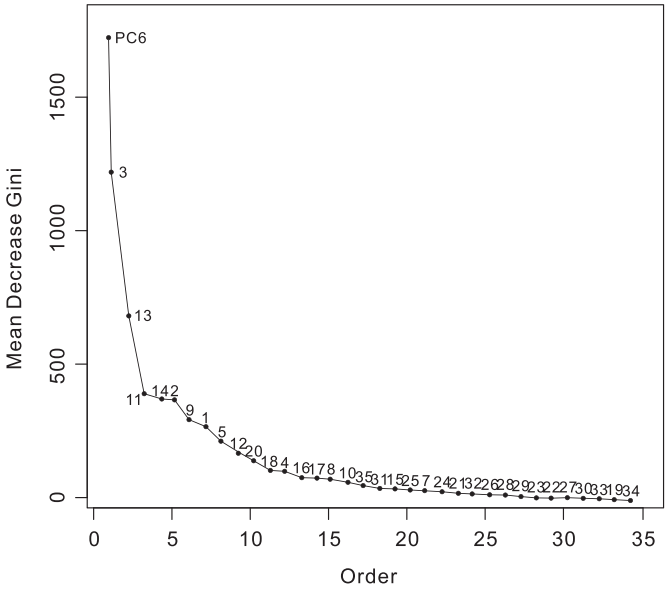

Fig. 7. Mean Decrease Gini showing the importance of the PCs for RF. The numbers are the numbers of PCs.

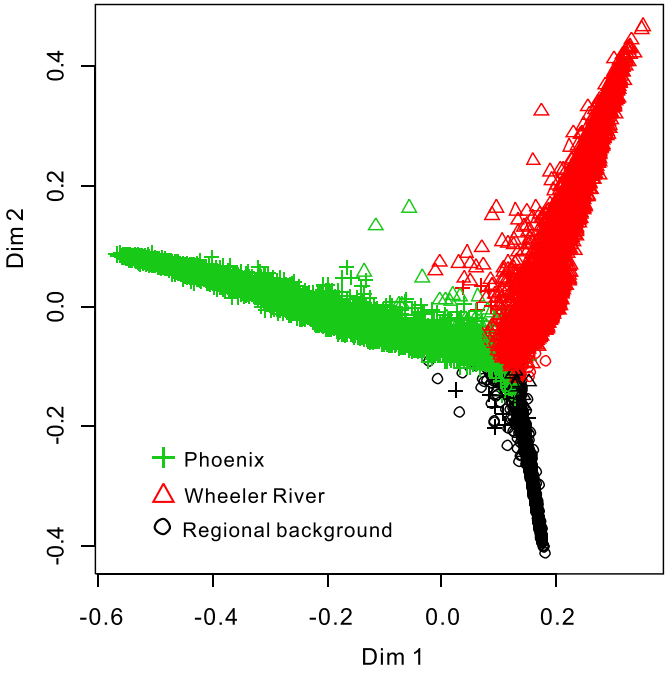

Fig. 8. MDS plot of RF classification. Dim = dimension. For each sample, the color represents the predicted classification and the symbol represents the actual classification.

Table 4
Average oob accuracies derived from the RF after five repetitions.

Data sets	Predicted			Accuracy rate	Total accuracy rate
	Regional background	Phoenix	Wheeler River		
Regional background	2099	13	63	96.5%	98.4%
Wheeler River	30	48	6227	98.7%	
Phoenix	8	4559	52	98.8%	

sandstones with very minor overlap (Fig. 6; Table 3): Class Phoenix, Class Wheeler River, and Class Regional background. The overall discrimination shows high total accuracy rate of 95.5% (Table 3). Note that Class Phoenix constitutes the majority of sandstones overlying Phoenix deposit and several sandstones in Wheeler River and minor number of sandstones from regional background (Table 3).

5.3. Random forest

In this study, the RF method uses all PCs of the PCA conducted for LDA as variables and provides ranking of the predictive power of each input PC used for the RF classification. The *mtry* was set to 6 and *ntree* set to 1000. Mean Decrease Gini (Fig. 7) shows that PC6, PC3, PC13, PC11, PC14, PC2, PC9 and PC1 are the best classifiers. Multi-dimensional scaling (MDS) plot of RF (Fig. 8) and Table 4 show that the RF yields more refined discrimination of the 3 classes with a total accuracy rate of 98.4% (average value of 5 repetitions) compared to the accuracy using LDA (95.5%). In RF, the Class Phoenix is composed of 4559 sandstone samples that overly the Phoenix deposit, 48 sandstone samples in Wheeler River property and 13 sandstone samples from the regional background (Table 4).

6. Discussion

6.1. Elements associated with U and their spatial distribution

The Wheeler River data show that U is positively associated with REEs-Y-Cu-Na-Zn-W-Pb-Co-Cr-Sc-Mo-V-Ni-B-Mg and inversely with K-Rb-Fe-Th-Nb-Ti-Mn-Al-Ta-Sr-P-Sn-Li-Ba. The elemental assemblages are very similar to those of the sandstone samples above the Phoenix deposit reported by Chen et al. (2017). The similarity of the element assemblages in Wheeler River and Phoenix data sets suggests that the uraniferous hydrothermal activity was extensive beyond the sandstones directly above the deposit, and left macroscopic as well as cryptic alteration in the sandstones > 500 m from the deposit. The Wheeler River and Phoenix data sets show that the concentrations of elements positively associated with U, such as HREEs + Y and MgO, are higher in the majority of samples than those in the regional data set, although the latter shows a very large variation with few high values of outliers (Fig. 9A and B). As reported by Chen et al. (2017), these elements associated with U, including HREEs + Y and MgO (Fig. 9C and D), show high values directly above the deposit. The HREEs + Y form a well-defined “chimney-like” distribution pattern (Fig. 9C). On the other hand, the spatial distribution of the aforementioned elements in sandstones in barren areas does not show such ‘chimney-like’ pattern (Chen et al., 2017).

The PCA of regional background data set shows an elemental assemblage with U, but is different from that of the Wheeler River data set. In the regional dataset, U is strongly associated with Th-Ti-Hf-Zr-P-HREEs (Fig. 4A). This suggests phosphate minerals (xenotime, monazite, APS minerals), zircon and Fe-Ti oxides are possible hosts of U. Xenotime, monazite, and APS minerals are common in sandstones in the Athabasca Basin (e.g., Normand, 2014; Mwenifumbo and Bernius, 2007). However, a biplot of PC1 and PC3 shows that U is not closely associated with P and REEs (Fig. 4B). This suggests that REE minerals and phosphates are not major hosts of U but that U is hosted in zircon and Fe-Ti oxides heavy mineral bands containing Fe-Ti oxides, and zircon.

6.2. Implication of exploration in eastern Athabasca Basin

The elements positively associated with U in Wheeler River data set include REE, Na and B. Since Na and B are soluble elements in aqueous fluids, these elements are not concentrated during sedimentary

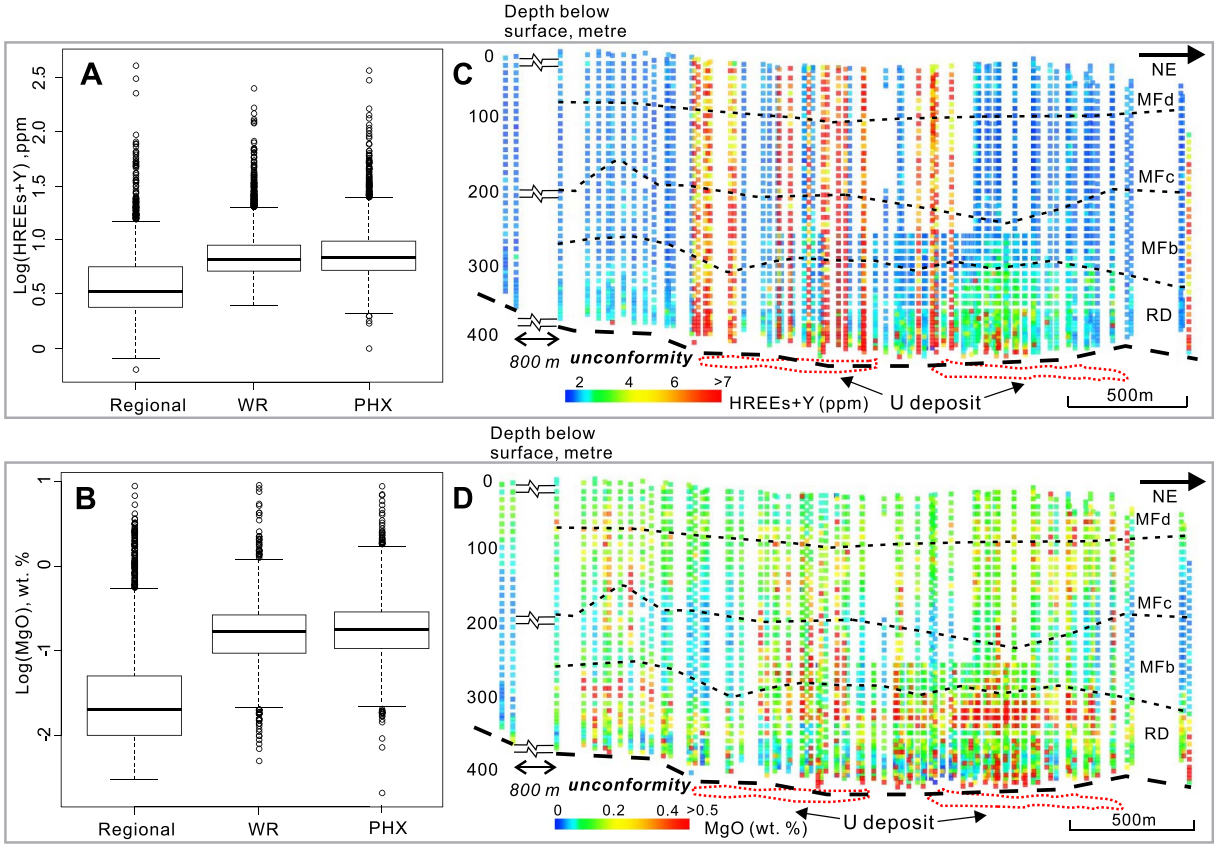

Fig. 9. A and B. Box-and-whisker plots of (HREEs + Y) and MgO concentrations in the regional, Wheeler River and Phoenix data sets separately. WR = Wheeler River, PHX = Phoenix. C and D. Spatial distribution of the (HREEs + Y) and MgO concentrations (after Chen et al., 2017). The sample locations are projected on a vertical plane along the strike of the ore bodies, shown in Fig. 2A. Each square on the plot represents one drill core sample. The data are not continuously plotted because of missing data (see text). Vertical exaggeration is 2×. Note that two DDHs in the left side of Fig. 9C and D are over 800 m from the rest of DDHs.

processes. Instead, they occur in hydrothermal alteration minerals, such as dravitic tourmaline, which have been identified in sandstones in the study area (Roscoe, 2015; O'Connell et al., 2015). Therefore, the distribution of sandstone samples containing high concentrations of the elements associated with U may indicate favorable areas for exploration.

The elements associated with U in sandstones in Wheeler River property are similar to those overlying the Phoenix deposit reported by Dann et al. (2014) and Chen et al. (2017), but their concentrations in the property are less than those over the ore (Table 1; Chen et al., 2017). This indicates that most sandstones in Wheeler River Property contain less alteration minerals than those overlying the Phoenix deposit. The different degrees of alteration likely resulted in separation of the two data sets into two classes by LDA and RF. For both classification methods, there are several samples from Wheeler River property that are classified as Phoenix Class (Tables 3 and 4), indicating that these samples are altered in a style similar to samples overlying the Phoenix deposit, and contain more alteration minerals compared with other sandstone samples in the property. Some sandstones are visibly altered, but some are microscopically altered. The locations of such cryptically altered sandstones identified by LDA and RF are shown in Figs. 10 and 11. These sandstone samples are mostly located ~1 km northeast of the Phoenix deposit and above the Gryphon deposit, reflecting a clear footprint of uraniferous hydrothermal activity in these areas. The strong footprint also occurs in the northeast part of the area (2–3 km from the deposit) above a major basement fault and the main quartzite ridge (Fig. 2), where weak mineralization has been identified at the unconformity (Denison Mines Corp., 2017). Basement faults have been suggested to be major conduits for uraniferous hydrothermal fluids (McGill et al., 1993; Jefferson et al., 2007; Adlakha and Hattori, 2015). Therefore, it is likely that basement fluids flowed through the faults and upwards into sandstones, and dispersed elements in the sandstones (Chen et al., 2017; Adlakha et al., 2017).

6.3. Comparison of LDA and RF classification

Linear discriminant analysis provides computational simplicity of large data sets and it has been extensively used for classification and prediction purposes, in the fields of biological, sociological and software engineering sciences. This analysis can be performed with widely available statistical programs, such as R (Package MASS), MATLAB (Package ClassificationDiscriminant), SAS (Function PROC DISCRIM) and SPSS (Function Discriminant Analysis). The analytical method of RF is a recently developed machine learning algorithm. Many studies suggest that RF yields a better discrimination of compositional data over other methods (Cracknell and Reading, 2014; O'Brien et al., 2015). Several recent studies, including Cracknell and Reading (2014), Carranza and Laborte (2015), O'Brien et al. (2015) and Harris and

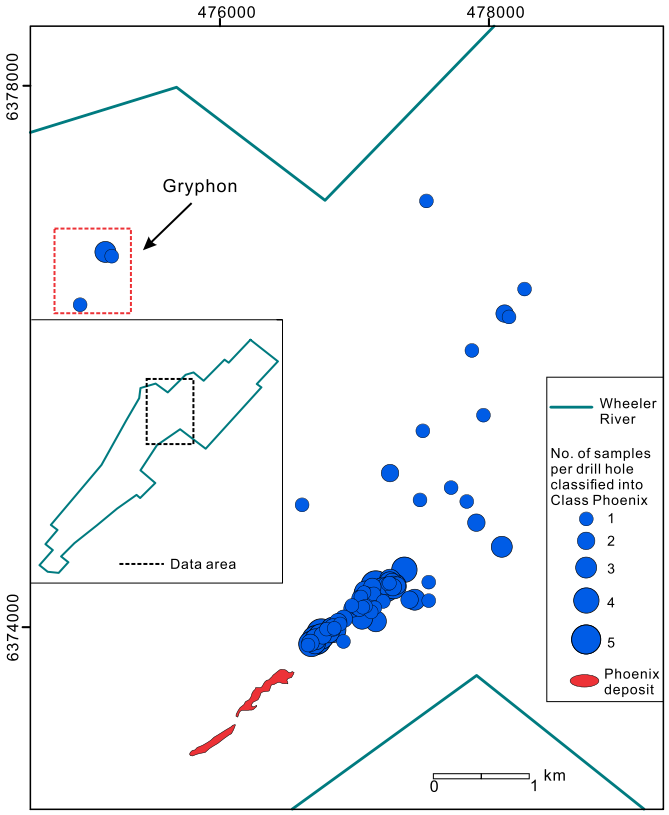

Fig. 10. Locations of the Wheeler River DDHs containing altered sandstone samples identified by LDA. The size of symbol reflects the number of altered sandstone samples in a DDH.

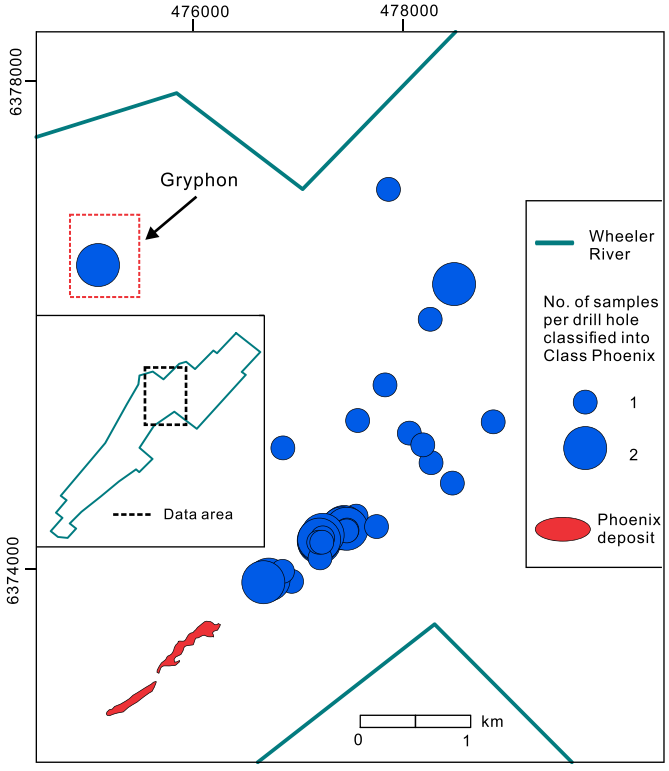

Fig. 11. Locations of the Wheeler River DDHs containing altered sandstone samples identified by RF. The size of symbol reflects the number of altered sandstone samples in a DDH.

Grunsky (2015), used RF and suggested its usefulness in mineral exploration and geological mapping.

In this study, both LDA and RF yielded very good discrimination of data using PCs as variables. Although LDA is faster in computation, RF method offers a number of advantages over LDA. First, the receiver operating characteristic curves and precision/recall curves (Fig. 12) indicate that both RF and LDA yielded very accurate classification. A high area under the receiver operating characteristic curve represents high true positive rate and low false positive rate, and under a precision/recall curve represents both high recall and high precision, where high precision relates to a low false positive rate, and high recall relates to a low false negative rate. Therefore, the higher values of area under curves of RF indicate that RF is a better method than LDA in this study. The accuracy assessments show that RF-based classification yielded 98.4% accuracy rate, whereas LDA gave 95.5% accuracy rate (Tables 3, 4). Although the difference of 3% in the accuracy rates for the two methods appears small, this is equivalent to over 390 samples. More samples are misclassified with LDA. In exploration, this difference may lead to incorrect assessment of areas and affect the strategy in targeting favorable areas. Second, RF does not require cross-validation or a separate test set to get an unbiased estimate of the test set error, because RF performs internal cross-validation through bootstrapping. Third, RF requires little user input (*mtry* and *ntree*). Fourth, it is not necessary to examine the importance of input variables before RF because this algorithm automatically gives estimates of what variables are important in the classification. Additional advantages of RF are described by many previous studies (Breiman, 2001; Cracknell and Reading, 2014; Harris and Grunsky, 2015). Based on the benefits described above, we suggest RF for classification of compositional data of sandstones in U exploration. We also recommend application of at least one additional classification method, such as LDA to verify the classification results.

7. Conclusions

(1) PCA of lithogeochemistry of sandstone samples from Wheeler River property shows that U is positively associated with REEs-Y-Cu-Na-Zn-W-Pb-Co-Cr-Sc-Mo-V-Ni-B-Mg. The element assemblage is similar to that associated with U in sandstones overlying the Phoenix U deposit as reported by Chen et al. (2017). The data suggests uraniferous hydrothermal activity affected sandstones not only directly above the U deposit but also in the entire Wheeler River property;

(2) The elemental assemblage associated with U in barren areas is different from that in the Wheeler River property. The assemblage indicates that U is hosted by detrital minerals, such as zircon and Fe-Ti oxides. The findings from this study demonstrate that the sandstones in mineralized and unmineralized areas are geochemically distinct;

(3) PCA is able to identify elemental assemblages associated with U, thus it is helpful in detecting the geochemical signature overlying deeply buried U deposits. LDA and RF using elemental assemblages are effective in identifying the areas underlain by sandstones affected by uraniferous hydrothermal activity. The methodology used and the elemental assemblages reported in this study may be useful in exploration for deeply buried U deposits in Proterozoic basins worldwide;

(4) Classification of lithogeochemistry of sandstones is successfully achieved by LDA or RF, but receiver operating characteristic and precision/recall curves and the values of area under the curve suggest that RF method offers better accuracy and several additional advantages. Therefore, we suggest that RF is a preferred statistical technique to LDA for compositional discrimination.

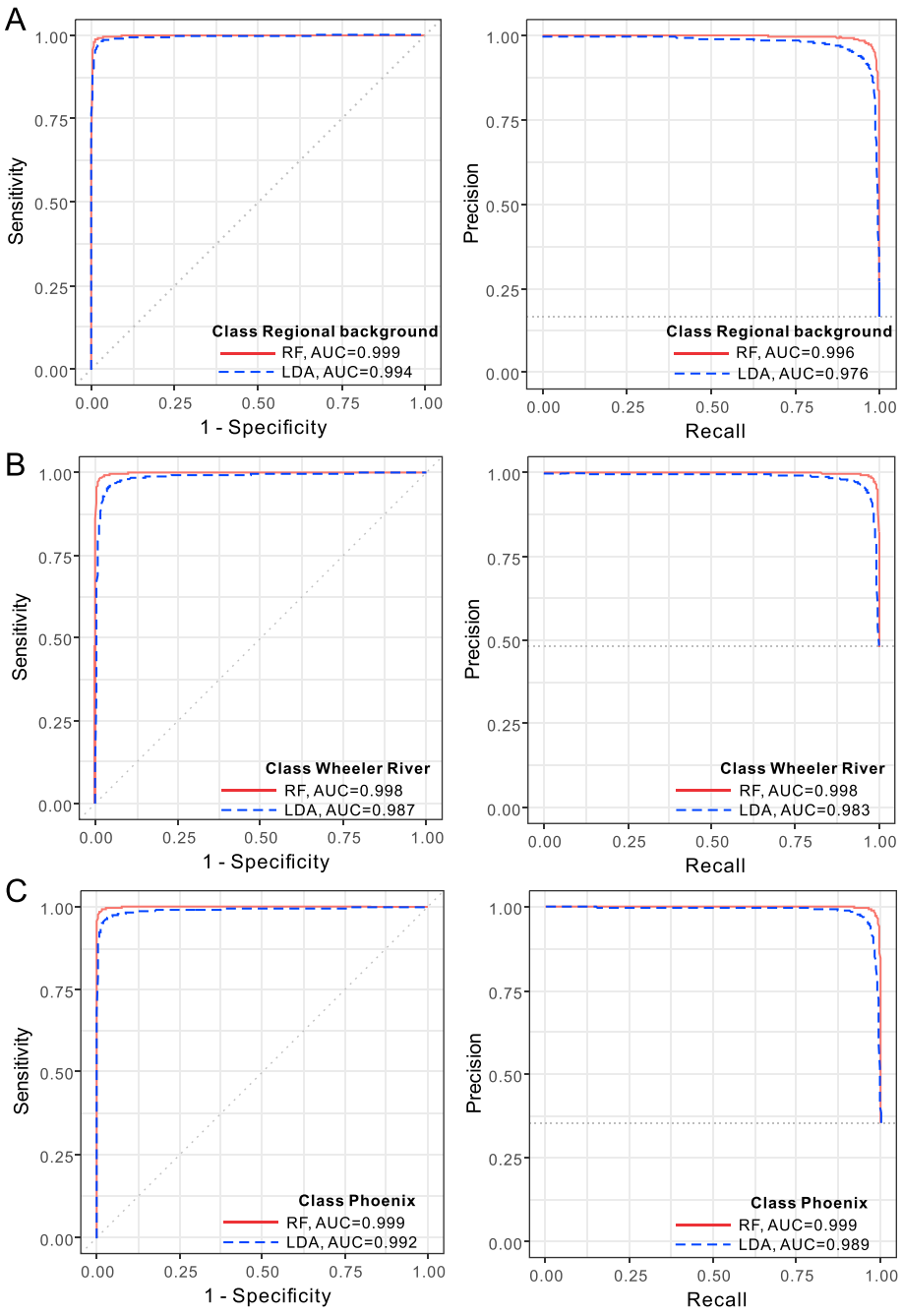

Fig. 12. Receiver operating and precision/recall curves for RF and LDA classifications for Class Regional background (A), Class Wheeler River (B) and Class Phoenix (C) separately.

Acknowledgements

This study is a part of PhD project by S.C. at the University of Ottawa. Denison Mines Corporation provided the lithogeochemical data of Wheeler River Property to the research team at the University of Ottawa. We are grateful to the Denison Mines Corporation for providing generous logistic support for our field work. Special thanks extend to Lawson Forand, Dale Verran, Chad Sorba, and Yongxing Liu. This research project was funded by a grant to K.H. from Natural Resources Canada through the TGI-4 Uranium Ore System program, which was led by Eric Potter of the Geological Survey of Canada. Comments from Eric Potter and an anonymous reviewer greatly improved the clarity of the manuscript.

Appendix A. Supplementary data

Supplementary data to this article can be found online at https://doi.org/10.1016/j.gexplo.2018.01.026.

References

Adlakha, E.E., Hattori, K., 2015. Compositional variation and timing of aluminum phosphate-sulfate minerals in the basement rocks along the P2 fault and in association with the McArthur River uranium deposit, Athabasca Basin, Saskatchewan, Canada. Am. Mineral. 100, 1386–1399.

Adlakha, E.E., Hattori, K., Davis, W.J., Boucher, B., 2017. Characterizing fluids associated with the McArthur River U deposit, Canada, based on tourmaline trace element and stable (B, H) isotope compositions. Chem. Geol. 466, 417–435.

Aitchison, J., 1986. The Statistical Analysis of Compositional Data. Chapman and Hall, London.
Analytics Vidhya Content team, 2016. A complete tutorial on tree based modeling from scratch (in R & Python). https://www.analyticsvidhya.com/blog/2016/04/complete-tutorial-tree-based-modeling-scratch-in-python/ (Accessed Jan 5, 2018).
Bosman, S.A., Card, C.D., MacKnight, S.G., Boulanger, S., 2012. The Athabasca Basin ore-systems project: an update on geochemistry, spectral data, and core logging. In: Summary of Investigations 2012, Volume 2, Saskatchewan Geological Survey, Sask. Ministry of the Economy, Misc. Rep. 2012-4.2, Paper A-5.
Breiman, L., 2001. Random forests. Mach. Learn. 45, 5–32.
Carranza, E.J.M., 2008. Geochemical Anomaly and Mineral Prospectivity Mapping in GIS. vol. 11 Elsevier, Amsterdam.
Carranza, E.J.M., Laborte, A.G., 2015. Random forest predictive modeling of mineral prospectivity with small number of prospects and data with missing values in Abra (Philippines). Comput. Geosci. 74, 60–70.
Chandrajith, R., Dissanayake, C.B., Tobschall, H.J., 2001. Application of multi-element relationships in stream sediments to mineral exploration: a case study of Walawe Ganga Basin, Sri Lanka. Appl. Geochem. 16, 339–350.
Chen, S., Hattori, K., Grunsky, E.C., 2016. Multivariate statistical analysis of the REE-mineralization of the Maw Zone, Athabasca Basin, Canada. J. Geochem. Explor. 161, 98–111.
Chen, S., Hattori, K., Grunsky, E.C., 2017. Multi-element statistical evidence for uraniferous hydrothermal activity in sandstones overlying the Phoenix uranium deposit, Athabasca Basin, Canada. Mineral. Deposita. http://dx.doi.org/10.1007/s00126-017-0756-2. (in press).
Cheng, Q., Bonham-Carter, G., Wang, W., Zhang, S., Li, W., Qinglin, X., 2011. A spatially weighted principal component analysis for multi-element geochemical data for mapping locations of felsic intrusions in the Gejiu mineral district of Yunnan, China. Comput. Geosci. 37, 662–669.
Chork, C.Y., Rousseeuw, P.J., 1992. Integrating a high-breakdown option into discriminant analysis in exploration geochemistry. J. Geochem. Explor. 43, 191–203.
Clarke, D.B., Reardon, N.C., Chatterjee, A.K., Gregoire, D.C., 1989. Tourmaline composition as a guide to mineral exploration; a reconnaissance study from Nova Scotia using discriminant function analysis. Econ. Geol. 84, 1921–1935.
Cracknell, M.J., Reading, A.M., 2014. Geological mapping using remote sensing data: a comparison of five machine learning algorithms, their response to variations in the spatial distribution of training data and the use of explicit spatial information. Comput. Geosci. 63, 22–33.
Dann, J., Hattori, K., Potter, E.G., Sorba, C., 2014. Discrimination of elemental assemblages in the alteration halo of the phoenix deposit, Saskatchewan, through applied GIS. In: Geological Survey of Canada, Open File Report 7463.
Denison Mines Corp, 2017. Wheeler river property. http://www.denisonmines.com/s/Wheeler_River.asp (Accessed April 30, 2017).
Earle, S., Sopuck, V., 1989. Regional lithogeochemistry of the eastern part of the Athabasca Basin uranium province, Saskatchewan. In: Muller-Kahle, E. (Ed.), Uranium Resources and Geology of North America: International Atomic Energy Agency, Technical Document TECDOC-500, pp. 263–269.
Filzmoser, P., Hron, K., Templ, M., 2012. Discriminant analysis for compositional data and robust parameter estimation. Comput. Stat. 27, 1–20.
Gamelin, C., Sorba, C., Kerr, W., 2010. The discovery of the Phoenix deposit: a new high-grade Athabasca Basin unconformity-type uranium deposit, Saskatchewan, Canada. In: Saskatchewan Geological Survey Open House 2010. vol. 17 (Abstract).
Grunsky, E.C., 2010. The interpretation of geochemical survey data. Geochem.: Explor., Environ., Anal. 10, 27–74.
Grunsky, E.C., Mueller, U.A., Corrigan, D., 2014. A study of the lake sediment geochemistry of the Melville Peninsula using multivariate methods: applications for predictive geological mapping. J. Geochem. Explor. 141, 15–41.
Guffey, S., Piercey, S., Ansdell, K., Kyser, K., Kotzer, T., Zaluski, G., 2015. Potential pathfinder elements: footprint of 3D lithogeochemistry of the millennium unconformity-type uranium deposit, Athabasca Basin, Saskatchewan. In: 27th International Applied Geochemistry Symposium, Tucson, USA, (Abstract).
Harris, J.R., Grunsky, E.C., 2015. Predictive lithological mapping of Canada's north using random forest classification applied to geophysical and geochemical data. Comput. Geosci. 80, 9–25.
Hoeve, J., Quirt, D.H., 1984. Mineralization and host rock alteration in relation to clay mineral diagenesis and evolution of the middle-Proterozoic Athabasca Basin, northern Saskatchewan, Canada. In: Saskatchewan Research Council Technical Report. 187.
Hron, K., Templ, M., Filzmoser, P., 2010. Imputation of missing values for compositional data using classical and robust methods. Comput. Stat. Data Anal. 54, 3095–3107.
Jefferson, C.W., Thomas, D.J., Gandhi, S.S., Ramaekers, P., Delaney, G., Brisbin, D., Cutts, C., Quirt, D., Portella, P., Olson, R.A., 2007. Unconformity-associated uranium deposits of the Athabasca Basin, Saskatchewan and Alberta. In: Goodfellow, W. (Ed.), Mineral Deposits of Canada: A Synthesis of Major Deposit-types, District Metallogeny, the Evolution of Geological Provinces, and Exploration Methods. Special Publication No. 5 Geological Association of Canada, Mineral Deposits Division, pp. 273–305.
Kotzer, T., Kyser, T.K., 1995. Fluid history of the Athabasca Basin and its relation to diagenesis, uranium mineralization and paleohydrology. Chem. Geol. 120, 45–89.
Liaw, A., Wiener, M., 2002. Classification and regression by randomForest. R News 2, 18–22.
Mao, M., Rukhlov, A.S., Rowins, S.M., Spence, J., Coogan, L.A., 2016. Apatite trace element compositions: a robust new tool for mineral exploration. Econ. Geol. 111, 1187–1222.
McGill, B., Marlatt, J., Matthews, R., Sopuck, V., Homeniuk, L., Hubregtse, J., 1993. The P2 north uranium deposit Saskatchewan, Canada. Explor. Min. Geol. 2, 321–331.
McKinley, J.M., Grunsky, E., Mueller, U., 2017. Environmental monitoring and peat assessment using multivariate analysis of regional-scale geochemical data. Math. Geosci. http://dx.doi.org/10.1007/s11004-017-9686-x. (in press).
Mwenifumbo, C.J., Bernius, G.R., 2007. Crandallite-group minerals: host of thorium enrichment in the eastern Athabasca basin, Saskatchewan. In: Jefferson, C.W., Delaney, G. (Eds.), EXTECH IV: Geology and Uranium Exploration TECHnology of the Proterozoic Athabasca Basin, Saskatchewan and Alberta. Geological Survey of Canada, Bulletin 588pp. 521–532.
Neff, H., 1994. RQ-mode principal components analysis of ceramic compositional data. Archaeometry 36, 115–130.
Normand, C., 2014. Rare earths in Saskatchewan: mineralization types, settings, and distributions; Saskatchewan ministry of the economy. In: Saskatchwan Geological Survey Report. 264.
O'Brien, J.J., Spry, P.G., Nettleton, D., Xu, R., Teale, G.S., 2015. Using random forests to distinguish gahnite compositions as an exploration guide to Broken Hill-type Pb–Zn–Ag deposits in the Broken Hill domain, Australia. J. Geochem. Explor. 149, 74–86.
O'Connell, I., Hattori, K., Chen, S., Adlakha, E.E., Sorba, C., 2015. Characterization of Tourmaline From the Maw Zone, Gryphon Zone and Sandstones Above the Phoenix Uranium Deposits, Athabasca. Scientific Presentation 37 Geological Survey of Canada, Basin, Saskatchewan, Canada.
R Core Team, 2013. R: A Language and Environment for Statistical Computing. R Foundation for Statistical Computing, Vienna, Austria.
Ramaekers, P., 1979. Stratigraphy of the Athabasca Basin. In: Summary of Investigations 1979, Saskatchewan Geological Survey. Saskatchewan Department of Mineral Resource Miscellaneous Report 79-10, pp. 154–160.
Ramaekers, P., Jefferson, C.W., Yeo, G.M., Collier, B., Long, D.G.F., Drever, G., Wheatley, K., 2007. Revised geological map and stratigraphy of the Athabasca Group, Saskatchewan and Alberta. In: Jefferson, C.W., Delaney, G. (Eds.), EXTECH IV: Geology and Uranium Exploration TECHnology of the Proterozoic Athabasca Basin, Saskatchewan, and Alberta. Geological Survey of Canada, Bulletin 588pp. 155–190.
Reid, K.D., Ansdell, K., Jiricka, D., Witt, G., Card, C., 2014. Regional setting, geology, and paragenesis of the centennial unconformity-related uranium deposit, Athabasca Basin, Saskatchewan, Canada. Econ. Geol. 109, 539–566.
Roscoe, W., 2015. Technical report on a mineral resource estimate update for the Phoenix uranium deposit, Wheeler River Project, eastern Athabasca Basin, northern Saskatchewan, Canada. In: NI 43-101 Report.
Sopuck, V.J., de Carle, E.M., Cooper, B., 1983. The application of lithogeochemistry in the search for unconformity-type uranium deposits, northern Saskatchewan, Canada. J. Geochem. Explor. 19, 77–99.
Templ, M., Filzmoser, P., Reimann, C., 2008. Cluster analysis applied to regional geochemical data: problems and possibilities. Appl. Geochem. 23, 2198–2213.
Templ, M., Hron, K., Filzmoser, P., 2010. robCompositions: robust estimation for compositional data. In: Manual and Package, Version 1.3.3.
Venables, W., Ripley, B., 2002. Modern Applied Statistics Using S. Springer, New York.
Wright, D.M., Potter, E.G., Comeau, J.S., 2015. Athabasca Basin Uranium Geochemistry Database v.2. Geological Survey of Canada, Open File Report 7792.
Zuo, R., 2011. Identifying geochemical anomalies associated with Cu and Pb–Zn skarn mineralization using principal component analysis and spectrum–area fractal modeling in the Gangdese Belt, Tibet (China). J. Geochem. Explor. 111, 13–22.